Moving atoms on surfaces: Impact of external parameters on required lateral force

J. Brand,* N. Néel, and J. Kröger
Institut für Physik, Technische Universität Ilmenau, D-98693 Ilmenau, Germany

(Received 11 October 2018; published 18 December 2018)

Combining scanning tunneling microscopy and atomic force spectroscopy the dependence of the lateral force to move single adsorbed atoms on surfaces on the temperature is explored. A decrease of the force with increasing temperature is observed for all atoms and surfaces investigated and may be captured in a simple model. Crossing the critical temperature as well as surmounting the critical magnetic field of a superconductor does not lead to discriminable changes in the lateral force.

DOI: 10.1103/PhysRevB.98.235420

I. INTRODUCTION

Manipulating matter atom by atom is undoubtedly one of the most fascinating capabilities of a scanning tunneling microscope (STM) and an atomic force microscope (AFM). The last three decades have witnessed a tremendous evolution in the fabrication of artificial assemblies, initiated by first observations of atom manipulation [1] and the controlled movement of single atoms [2], proceeding with the identification of different manipulation methods [3] and the construction of atom corrals [4–6], the realization of molecule cascades [7], atomic chains [8,9], and magnetic atom assemblies [10–14] to the autonomous assembly of nanostructures [15]. Many more works are summarized in excellent review articles [16–20].

The intriguing question concerning the force that is needed to move single atoms and molecules on surfaces was first answered in a seminal work for Co and CO on Pt(111) and Cu(111) [21]. The basic findings of this work revealed that forces strongly depend on the actual atom-surface combination and may differ by more than an order of magnitude. Forces during the displacement of more complex molecules were likewise reported [22–24].

The impetus to the work presented here arises from several aspects. First, the powerful method introduced in Ref. [21] should be applied to a variety of atom-surface combinations in order to rely on an increased data base. Second, experiments that have been reported so far were carried out at a single or at most at two temperatures. Therefore, the temperature dependence of the threshold force has not been explored in detail to date. In particular, for superconductors an effect in the threshold force may be expected for temperatures below and above the critical temperature (T_c) of the superconductor. Third, the superconducting state may be influenced by an external magnetic field and it is interesting to compare possible changes in the lateral force with those obtained in temperature-dependent experiments.

By applying the method of Ref. [21], the lateral threshold force to move single adsorbed atoms (adatoms), Pb on Pb(111), Co and Au atoms on Au(111), Co and Cu atoms on Cu(111), and its temperature dependence was studied in the work presented here. A simple model reproduces the behavior and unravels the interplay between the periodic surface potential, the tip-induced potential, and the lateral tip velocity. For Pb(111), an effect of the temperature below and above T_c as well as of an external magnetic field below and above the critical field (B_c) on the threshold force stays below the detection limit.

II. EXPERIMENT

The experiments were performed with a combined STM and AFM operated at low temperature (5.8 K) and in ultrahigh vacuum (10^{-9} Pa). Tips were fabricated from chemically etched PtIr wire that was further prepared by field emission in the vacuum recipient. The force probe is a tuning fork with stiffness $k = 1800$ N/m, resonance frequency $f_0 = 29.9$ kHz, quality factor $Q = 24\,000$ at 5.8 K, and a zero-to-peak amplitude of $A = 30$ pm. Clean and single-crystalline (111) surfaces of Pb, Au, Cu were obtained after repeated cycles of Ar^+ bombardment and annealing. While Pb (Au, Cu) atoms on Pb(111) [Au(111), Cu(111)] were transferred from the tip to the surface [25–28], Co atoms were deposited on Au(111) and Cu(111) at low temperature using an electron beam evaporator. The force spectroscopy experiments require the tip approach toward the adatom until manipulation distances are reached. For reliable and reproducible data acquisition care was taken to retain an invariant tip structure. Averages over 5 to 10 individual measurements for each adatom-surface combination are presented here. STM images were recorded at constant current with the bias voltage applied to the sample. Spectra of the differential conductance (dI/dV) were recorded by sinusoidally modulating the bias voltage (0.15 mV_{rms}, 4.1 kHz) and measuring the first harmonic of the current response with a lock-in amplifier. Temperature-dependent data were recorded by heating the cold sample by passing a current across a Zener diode operated in reverse direction. The magnetic field is obtained by passing a current through a superconducting coil. It is oriented along the surface normal.

*jonathan.brand@tu-ilmenau.de

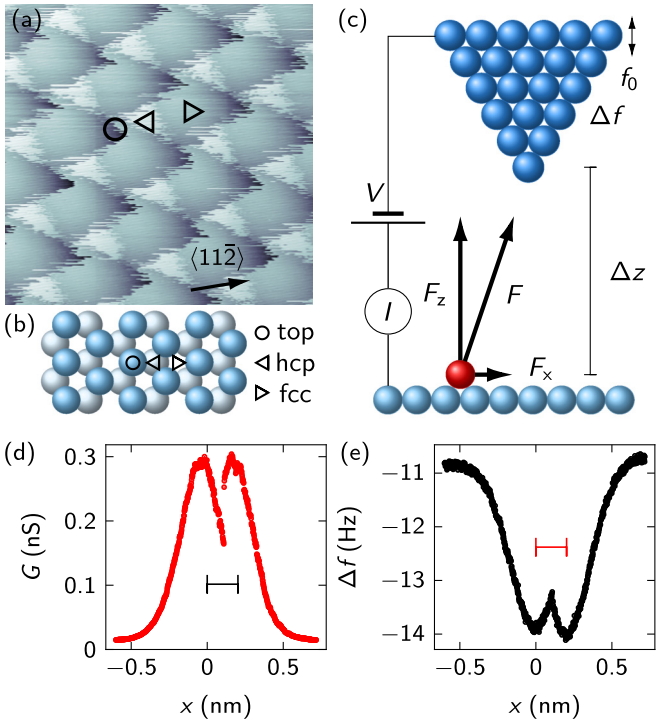

FIG. 1. (a) Atomically resolved STM image of Pb(111) that was obtained by dragging a single Pb atom with the tip across the surface (bias voltage $V = 1$ mV, tunneling current $I = 3$ nA). The different contrast is due to on-top (○), hcp (◁), and fcc (▷) lattice sites. The $\langle 11\bar{2}\rangle$ direction is indicated. (b) Sketch of first two Pb(111) lattice planes with indication of on-top, hcp, and fcc sites. (c) Illustration of the experimental setup that determines vertical (F_z) and lateral (F_x) forces. The distance between tip and surface is set by V and I. F_z is extracted from changes Δf in the resonance frequency f_0 of the oscillating tuning fork. (d) Conductance $G = I/V$ as the tip is scanned across a Pb adatom on Pb(111) at constant height (100 mV, 5.8 K). Prior to scanning the tip height was set at 100 mV, 56 nA. Subsequently the tip was approached by 195 pm. (e) Δf, simultaneously recorded with G in (d). The abrupt changes in (d) and (e) at $x \approx 0.11$ nm indicate the displacement of the adatom. The maxima (minima) of G (Δf) are separated by ≈0.20 nm (horizontal bar), which corresponds to the distance between hcp and fcc sites on Pb(111).

III. RESULTS AND DISCUSSION

In the force spectroscopy experiments to be discussed below the adatom is dragged between adjacent hexagonal close-packed (hcp) and face-centered cubic (fcc) surface lattice sites, which corresponds to the $\langle 11\bar{2}\rangle$ direction. The hcp-fcc direction may readily be determined from atomically resolved STM images [Fig. 1(a)]. Such data are routinely obtained by dragging adsorbed species across the surface [29,30]. The contrast in these topographic data reflects the propensity of the dragged atom to reside at on-top, hcp, and fcc sites [Fig. 1(b)]. In the course of dragging, the adatom tends to avoid on-top sites and jumps to adjacent hcp and fcc sites. Therefore, to maintain a constant current the tip-surface distance is decreased leading to a depression in the image at on-top sites [circle in Fig. 1(a)]. Moreover, a recent STM study showed by atomically resolved contact measurements that hcp sites exhibit the largest conductance followed closely by fcc sites, while on-top sites yield the lowest conductance [31]. These data are in line with the observations in Fig. 1(a). Similar data are available for the other investigated surfaces, Au(111) and Cu(111) [32].

In order to access the lateral force $\hat{F}_x$ that is required to move the adatom between adjacent hcp and fcc sites a previously introduced method [21] is used. The basic procedure is illustrated in Fig. 1(c). The tip-surface distance (Δz) is gradually decreased. At each distance, the adatom is imaged in the constant-height mode along the hcp-fcc direction and the spatial variation in the conductance ($G = I/V$, I: current, V: bias voltage) as well as changes in the resonance frequency (Δf) of the tuning fork are measured. An example of G and Δf is depicted in Figs. 1(d) and 1(e), respectively, for the threshold tip height, at which the adatom hops between adjacent hcp and fcc sites. The abrupt changes in G and Δf at $x \approx 0.11$ nm signal the displacement of the adatom. The distance between the maxima (minima) of G (Δf) is ≈0.20 nm, which matches well the hcp-fcc separation on Pb(111).

The resonance frequency change Δf is a measure of the vertical stiffness of the junction and may be converted into the vertical force F_z [Fig. 1(c)] [33]. To access the sought lateral force F_x, the vertical force has to be extracted from $\Delta f(x, z)$ for each lateral x and vertical z. It is then possible to obtain the interaction energy $E = -\int F_z \, dz$ and $F_x = -\partial E/\partial x$ for each x and z. These data are depicted in Fig. 2 for a Pb adatom on Pb(111) [32]. Particular care was taken to leave the tip apex invariant during a complete set of experiments since the actual tip termination was previously demonstrated to lead to different forces [21,24]. Figure 2(a) shows a set of $\Delta f(x, z)$ data acquired at 5.8 K with decreasing (top to bottom) tip-surface distance. The bottom curve abruptly stops at $x \approx -0.22$ nm and indicates the displacement of the adatom. The resulting vertical force is depicted in Fig. 2(b). At 5.8 K, its average value for moving the atom is $\hat{F}_z = -0.35 \pm 0.15$ nN. After integration of F_z the interaction energy E is obtained [Fig. 2(c)] from which F_x may be determined [Fig. 2(d)]. Its average value for displacing the adatom is $\hat{F}_x = 11.2 \pm 1.5$ pN. $\hat{F}_z$ was found to depend on the actual tip shape, while $\hat{F}_x$ stayed essentially invariant [32], which is in accordance with previous findings [21].

Table I summarizes $\hat{F}_z$ and $\hat{F}_x$ for all investigated adatoms and surfaces. $\hat{F}_x$ obtained for Co on Cu(111) at 6.7 K,

TABLE I. Summary of vertical ($\hat{F}_z$) and lateral ($\hat{F}_x$) threshold forces obtained for adatoms on diverse surfaces at the indicated temperatures. The forces and their uncertainty margins denote the, respectively, arithmetic mean and root-mean-square deviation of several measurements.

Adatom-substrate	$\hat{F}_z$ (nN)	$\hat{F}_x$ (pN)	T (K)
Pb-Pb(111)	-0.35 ± 0.15	11.2 ± 1.5	5.8
Au-Au(111)	-0.51 ± 0.11	34.0 ± 4.6	6.1
Co-Au(111)	-0.97 ± 0.27	30.7 ± 3.8	6.1
Cu-Cu(111)	-0.43 ± 0.16	38.2 ± 3.7	6.0
Co-Cu(111)	-0.26 ± 0.01	13.6 ± 0.3	6.7

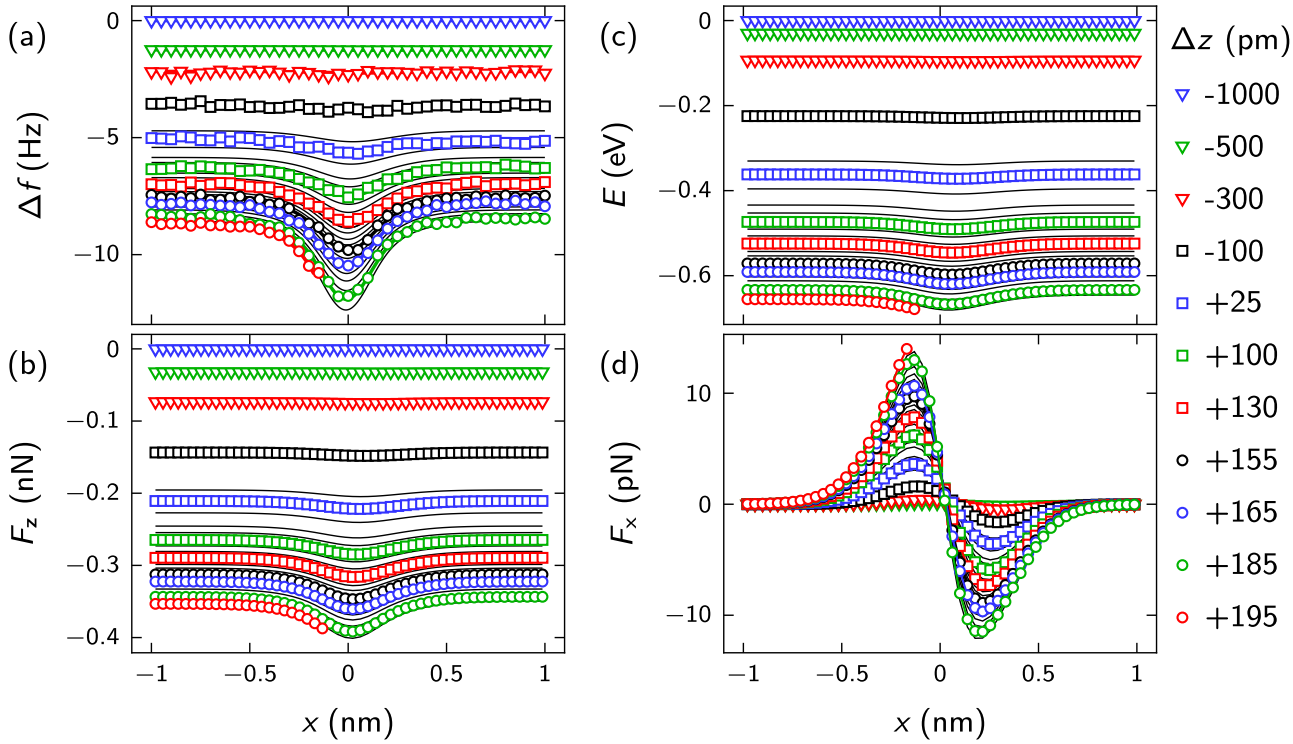

FIG. 2. AFM data of a single Pb adatom on Pb(111) as a function of the tip-surface distance (Δz) and the lateral position (x) acquired at 5.8 K. Vertical distance $\Delta z = 0$ pm is defined by feedback loop parameters 100 mV and 56 pA. The tip-surface distance decreases for -1000 pm $\leqslant \Delta z \leqslant 195$ pm. The adatom is located at $x = 0$ nm. (a) Resonance frequency variation Δf and (b) resulting vertical force F_z upon decreasing (from top to bottom) the tip-surface distance. (c) Interaction energy $E = -\int F_z \, dz$ and (d) lateral force $F_x = -\partial E/\partial x$. Symbols in (a) depict raw data. For evaluating F_z, E, F_x smoothed Δf data were used. In all panels, black lines are additional data, which are not displayed as symbols for clarity.

13.6 ± 0.3 pN, is in good agreement with previous results [21]. Moreover, for moving a single Pb adatom on Pb(111) a force is required that is more than three times lower than observed for Au adatoms on Au(111) and Cu adatoms on Cu(111). This striking observation reflects the different bonding characters. Bonding of Pb atoms to Pb(111) occurs primarily via weak sp^3 bonds [34] while the Au-Au(111) and Cu-Cu(111) bonding is dominated by robust s-d hybridization [35]. A possibly lower $\hat{F}_x$ for Au-Au(111) compared to Cu-Cu(111) may be rationalized in terms of the higher elasticity of Au atom chains [25,27], which is due to relativistic corrections for $5d$ elements [36]. The larger $\hat{F}_x$ for moving a single Co atom on Au(111) than on Cu(111) may be explained by calculated binding energies. Co residing at hcp and fcc sites of Au(111) exhibits a binding energy of $\approx$4.1 eV [37], while it is only $\approx$3.2 eV for Co on Cu(111) [38].

In a next step the temperature dependence of $\hat{F}_x$ was explored in a range 5.8 K $\leqslant T \leqslant$ 10 K; that is, data sets of Fig. 2 were acquired at different temperatures. The results are presented in Fig. 3. The approximate average slope ranges from ≈ -2 pN/K to ≈ -3 pN/K and matches observations reported for CO molecules on Cu(111) on the basis of two temperatures, -1.7 pN/K [24]. Within the uncertainty margin all adatoms on all surfaces exhibit a decrease of $\hat{F}_x$ with increasing T. Superconducting and normal-metal state of Pb(111) are best visualized by, respectively, the presence and absence of the Bardeen-Cooper-Schrieffer (BCS) energy gap [39] in dI/dV spectroscopy. The inset to Fig. 3 shows representative dI/dV spectra obtained for $T < T_c$ and $T > T_c$.

To describe the temperature behavior of $\hat{F}_x$ we are led by the idea that thermal activation assists the adatom in moving from one lattice site to the other and, concomitantly, reduces the lateral force $\hat{F}_x$ with increasing T. The rate of changing the adsorption site obeys an Arrhenius law [40,41], $\nu = \nu_0 \cdot \exp(-\beta E_b)$ with ν the transition rate, ν_0 the attempt rate, E_b the energy barrier, and $1/\beta = k_B T$ (k_B: Boltzmann constant). For E_b, the total energy landscape, $E = E_s + E_t$, has to be considered, where $E_s = -E_{s,0}/2 \cdot \cos(2\pi x/a)$ is the periodic surface energy with spatial period a, and $E_t = -E_{t,0} \cdot \exp[-(x - x_t)^2/w^2]$ denotes the tip-adatom interaction energy modeled as a Gaussian with maximum at the tip position x_t and width w.

According to the illustration in Fig. 4(a), E_b is the energy barrier between the adsorption site and the energetically most favorable site below the tip apex. The tip is moved across the adatom with a velocity v_x; that is, in the spatial interval Δx the tip stays a time $\Delta t = \Delta x/v_x$. This time may be compared with the mean time between two hopping events of the adatom, $\Delta\tilde{t} = 1/\nu = 1/\nu_0 \cdot \exp(\beta E_b)$. The tip will drag the adatom if $\Delta\tilde{t} \leqslant \Delta t$. For $\Delta\tilde{t} = \Delta t$ the minimum energy barrier to be overcome is defined as $E_b^0 = \ln(\nu_0 \Delta t)/\beta$, which serves as a temperature-dependent threshold barrier in the model. To determine the lateral force required to drag the adatom the algorithm proceeds as follows.

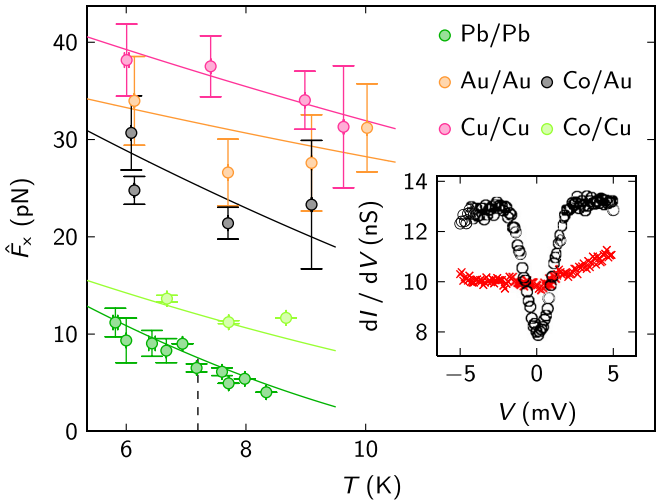

FIG. 3. Temperature dependence of $\hat{F}_x$ for the indicated adatom-surface combinations. The solid lines represent fits of a simple model to the data (see text). The vertical dashed line indicates the critical temperature of Pb(111), $T_c = 7.2$ K. Inset: dI/dV spectra at $T = 5.9$ K (circles) and $T = 8.0$ K (crosses). The feedback loop was disabled at 10 mV and 120 pA (circles), 100 pA (crosses).

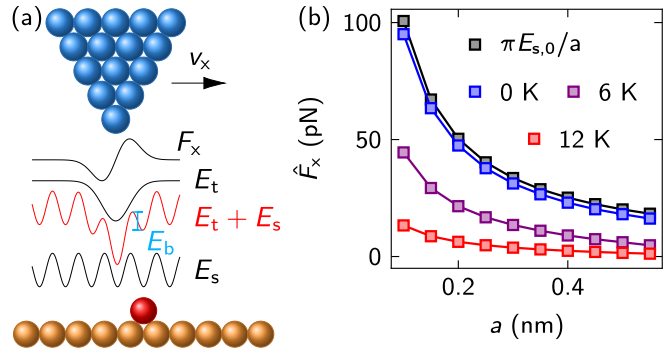

FIG. 4. (a) Ingredients of the model. The tip moves with velocity v_x across the surface and interacts with the adatom via the energy E_t. The adatom at $x = 0$ is subject to the superposition of E_t and the periodic lattice potential E_s. The adatom hops into the global minimum of $E_t + E_s$ if the barrier E_b is surmounted. The lateral force to move the adatom is obtained from $\hat{F}_x = -\partial E_t(x \approx 0)/\partial x$. (b) Lateral force $\hat{F}_x$ calculated within the model as a function of the lattice constant a and evaluated at the indicated temperatures. For $T = 0$ K the behavior is virtually identical with the variation previously suggested for the maximum lateral force in a sinusoidal lattice potential (top curve) [24].

With a given $E_{t,0}$ and $x_t < 0$ the tip is moved laterally towards the adatom at $x = 0$ in steps of Δx [42]. At each tip position E and E_b are evaluated. If $E_b > E_b^0$ then the tip is further approached laterally to the adatom until $E_b \leqslant E_b^0$ or $x_t \geqslant 0$. If the energy barrier E_b remains larger than E_b^0 for all x_t then the tip is moved back to its initial position where a new and larger $E_{t,0}$ is set, which in the experiments corresponds to a lowering of the tip-surface distance. Once $E_b \leqslant E_b^0$ the algorithm stops and evaluates the lateral force as $\hat{F}_x = -\partial E_t(x \approx 0)/\partial x$ [43]. This algorithm was repeated for different temperatures in the range 5.8 K $\leqslant T \leqslant$ 10 K and the least-squares fit results are plotted as solid lines in Fig. 3 [32]. Obviously, the experimentally observed behavior is reasonably well reproduced. In particular, the previously suggested behavior of the maximum lateral force in a sinusoidal lattice potential at 0 K [top curve in Fig. 4(b)] [24] is virtually identical with the results of the proposed model. We therefore conclude that the increased temperature thermally assists the adatom hopping and concomitantly reduces the lateral force to move the adatom.

Previously, quantum tunneling was identified as a contribution to the movement of adsorbed atoms and molecules on surfaces [7,44–49]. Its characteristic property is the temperature independence of the adsorbate hopping rate below a specific temperature, thereby deviating from the Arrhenius-type behavior. This temperature depends on the mass of the adsorbate and on the corrugation of the lattice potential [50,51]. For the experiments described here, adatom quantum tunneling is not significant since $\hat{F}_x$ does not level off below a specific temperature in the probed range. Rather, it increases monotonically with decreasing temperature (Fig. 3).

The $\hat{F}_x(T)$ data obtained for Pb(111) deserve particular attention since the probed temperature range contains T_c of Pb (vertical dashed line in Fig. 3). The data do not hint at an effect of the transition between the superconducting and normal-metal state neither on $\hat{F}_x$ nor on $\hat{F}_z$ and dissipation signals [32]. To further corroborate this result, the superconducting state of Pb(111) was influenced by an external magnetic field at constant temperature $T < T_c$. Figure 5 shows that within the uncertainty margins $\hat{F}_x$ remains virtually invariant below and above the critical field (dashed line). The suppression of the superconducting state above the critical field B_c is confirmed by the absence of the superconducting energy gap in dI/dV spectroscopy (inset to Fig. 5). $\hat{F}_z$ as well as the dissipation signal are unaffected, too [32]. Therefore, the

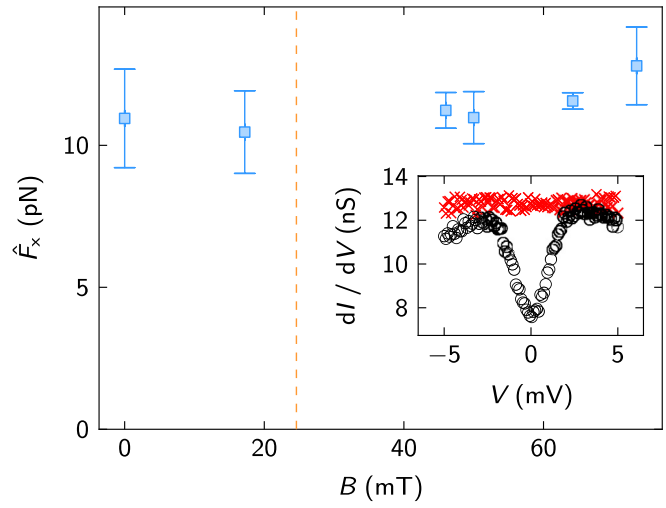

FIG. 5. $\hat{F}_x$ as a function of an external magnetic field applied to Pb(111) at 5.8 K. The vertical dashed line indicates the critical field at 5.8 K ($B_c = 25$ mT) above which the superconducting state collapses. Inset: dI/dV spectra of the BCS energy gap at external magnetic fields $B = 0$ T (circles) and $B = 46$ mT $> B_c$ (crosses). The feedback loop was disabled at 9.5 mV and 100 pA (circles), 120 pA (crosses).

transition between superconducting and normal-metal phases induced by an external magnetic field is not reflected by force and dissipation data.

How do these findings compare with previous results? Using a quartz crystal microbalance different dissipation signals were reported for adsorbates on Pb(111) upon crossing T_c (Ref. [52]) and B_c (Ref. [53]). These changes were attributed to differences in the electronic contribution to friction. In quartz crystal microbalance experiments an entire adsorbed film exerts a drag force on the electrons of the substrate, which gives rise to an electric current and ohmic losses for $T > T_c$. For $T < T_c$, the electronic friction vanishes since in the superconducting phase no electric field is present in the substrate.

In more recent pendulum AFM experiments the suppression of electronic friction on Nb films was reported upon reaching the superconducting state [54]. To observe clear signatures in the friction coefficient a cantilever with spring constant $k = 30$ mN/m was used. The interpretation of the experimental observations differs from Refs. [52,53]. Rather than inducing electric currents in the substrate [52,53], the oscillating cantilever was suggested to excite longitudinal acoustic surface waves [54]. Their attenuation due to coupling to normal-state electrons is reduced upon decreasing the temperature below T_c, which reflects the concomitantly decreasing normal-electron population.

In the aforementioned experiments [52–54], entire adsorbate films and substrate regions are involved in the measured dissipation signal, which represents a major difference to the experimental situation of moving a single atom from one lattice site to the other, as reported here. Moreover, in the pendulum AFM work [54] the cantilever spring constant was more than four orders of magnitude lower than in our tuning fork experiments. While such a low spring constant is susceptible to subtle changes in forces it would be detrimental to our approach due to the propensity of a snap to contact. Therefore, in the single-atom approach reported here, a possible effect of the transition between superconducting and normal-metal phases on the forces ($\hat{F}_x$, $\hat{F}_z$) and the dissipation signal is most likely too small to be detected with the current setup. Changes in the sliding friction force at T_c were estimated to be less than 1% [55], which is clearly below the uncertainty margins of the presented data (Figs. 3 and 5). A similar conclusion was drawn in another AFM experiment where changes of the vertical force around T_c measured by a tuning fork with a Cu tip on a Nb(110) sample were below the accuracy of the measurements [56].

IV. CONCLUSION

With state-of-the-art AFM, lateral threshold forces required to move single atoms on surfaces can be determined depending on the atom-surface combination and on external parameters. Increasing temperature thermally assists the manipulation process by reducing the threshold force. A possible effect of the superconducting and normal-metal state of Pb(111) on the threshold force to displace single Pb atoms stays below the detection limit. It will be interesting to see the potential impact of other condensed-matter phenomena, e.g., charge density waves and Kondo effect, or magnetic interactions on the lateral threshold force.

ACKNOWLEDGMENTS

Discussions with Dr. Nadine Hauptmann (Nijmegen) and financial support by the Deutsche Forschungsgemeinschaft through Grant No. KR 2912/12-1 are acknowledged.

[1] R. S. Becker, J. A. Golovchenko, and B. S. Swartzentruber, Nature **325**, 419 (1987).
[2] D. M. Eigler and E. K. Schweizer, Nature **344**, 524 (1990).
[3] J. A. Stroscio and D. M. Eigler, Science **254**, 1319 (1991).
[4] M. F. Crommie, C. P. Lutz, and D. M. Eigler, Science **262**, 218 (1993).
[5] J. Kliewer, R. Berndt, and S. Crampin, Phys. Rev. Lett. **85**, 4936 (2000).
[6] K.-F. Braun and K.-H. Rieder, Phys. Rev. Lett. **88**, 096801 (2002).
[7] A. J. Heinrich, C. P. Lutz, J. A. Gupta, and D. M. Eigler, Science **298**, 1381 (2002).
[8] S. Fölsch, P. Hyldgaard, R. Koch, and K. H. Ploog, Phys. Rev. Lett. **92**, 056803 (2004).
[9] N. Néel, R. Berndt, J. Kröger, T. O. Wehling, A. I. Lichtenstein, and M. I. Katsnelson, Phys. Rev. Lett. **107**, 106804 (2011).
[10] T. Jamneala, V. Madhavan, and M. F. Crommie, Phys. Rev. Lett. **87**, 256804 (2001).
[11] H. J. Lee, W. Ho, and M. Persson, Phys. Rev. Lett. **92**, 186802 (2004).
[12] N. Néel, J. Kröger, R. Berndt, T. O. Wehling, A. I. Lichtenstein, and M. I. Katsnelson, Phys. Rev. Lett. **101**, 266803 (2008).
[13] C. F. Hirjibehedin, C. P. Lutz, and A. J. Heinrich, Science **312**, 1021 (2006).
[14] M. Steinbrecher, R. Rausch, K. T. That, J. Hermenau, A. A. Khajetoorians, M. Potthoff, R. Wiesendanger, and J. Wiebe, Nat. Commun. **9**, 2853 (2018).
[15] R. J. Celotta, S. B. Balakirsky, A. P. Fein, F. M. Hess, G. M. Rutter, and J. A. Stroscio, Rev. Sci. Instrum. **85**, 121301 (2014).
[16] P. Avouris, Acc. Chem. Res. **28**, 95 (1995).
[17] G. Meyer, L. Bartels, and K.-H. Rieder, Superlattices Microstruct. **25**, 463 (1999).
[18] S.-W. Hla, J. Vac. Sci. Technol. B **23**, 1351 (2005).
[19] O. Custance, R. Perez, and S. Morita, Nat. Nanotechnol. **4**, 803 (2009).
[20] N. Pavliček and L. Gross, Nat. Rev. Chem. **1**, 0005 (2017).
[21] M. Ternes, C. P. Lutz, C. F. Hirjibehedin, F. J. Giessibl, and A. J. Heinrich, Science **319**, 1066 (2008).
[22] H.-Q. Mao, N. Li, X. Chen, and Q.-K. Xue, J. Phys.: Condens. Matter **24**, 084004 (2012).

[23] G. Langewisch, J. Falter, H. Fuchs, and A. Schirmeisen, Phys. Rev. Lett. **110**, 036101 (2013).
[24] M. Emmrich, M. Schneiderbauer, F. Huber, A. J. Weymouth, N. Okabayashi, and F. J. Giessibl, Phys. Rev. Lett. **114**, 146101 (2015).
[25] L. Limot, J. Kröger, R. Berndt, A. Garcia-Lekue, and W. A. Hofer, Phys. Rev. Lett. **94**, 126102 (2005).
[26] J. Kröger, H. Jensen, and R. Berndt, New J. Phys. **9**, 153 (2007).
[27] J. Kröger, N. Néel, A. Sperl, Y. F. Wang, and R. Berndt, New J. Phys. **11**, 125006 (2009).
[28] M. Müller, C. Salgado, N. Néel, J. J. Palacios, and J. Kröger, Phys. Rev. B **93**, 235402 (2016).
[29] M. Böhringer, W.-D. Schneider, and R. Berndt, Surf. Sci. **408**, 72 (1998).
[30] J. A. Stroscio and R. J. Celotta, Science **306**, 242 (2004).
[31] H. Kim and Y. Hasegawa, Phys. Rev. Lett. **114**, 206801 (2015).
[32] See Supplemental Material at http://link.aps.org/supplemental/10.1103/PhysRevB.98.235420 for atomically resolved topographic data of Au(111) and Cu(111) (Fig. S1), force spectroscopy data for Co and Au adatoms on Au(111) and for Co and Cu adatoms on Cu(111) (Figs. S2–S5), a visualization of the scattering and temperature dependence of $\hat{F}_x$ and $\hat{F}_z$ (Figs. S6 and S7), fit parameters and the behavior of the sum of squared residuals (Fig. S8), and dissipation signals as a function of temperature and magnetic field, which includes Ref. [57].
[33] J. E. Sader and S. P. Jarvis, Appl. Phys. Lett. **84**, 1801 (2004).
[34] J. C. Lian, Z. H. Cheng, Y. H. Jiang, Y. Y. Zhang, L. W. Liu, W. Ji, W. D. Xiao, S. X. Du, W. A. Hofer, and H.-J. Gao, Phys. Rev. B **81**, 195411 (2010).
[35] C.-G. Zhan, F. L. (Liu Fan), and Z.-M. Hu, Int. J. Quantum Chem. **32**, 13 (1987).
[36] M. R. Calvo, C. Sabater, W. Dednam, E. B. Lombardi, M. J. Caturla, and C. Untiedt, Phys. Rev. Lett. **120**, 076802 (2018).
[37] P. Yang, D. Li, V. Repain, C. Chacon, Y. Girard, S. Rousset, A. Smogunov, Y. J. Dappe, C. Barreteau, and J. Lagoute, J. Phys. Chem. C **119**, 6873 (2015).
[38] E. Zupanič, R. Žitko, H. J. P. van Midden, I. Muševič, and A. Prodan, Phys. Rev. Lett. **104**, 196102 (2010).
[39] J. Bardeen, L. N. Cooper, and J. R. Schrieffer, Phys. Rev. **108**, 1175 (1957).
[40] H. Brune, Surf. Sci. Rep. **31**, 125 (1998).
[41] J. Barth, Surf. Sci. Rep. **40**, 75 (2000).
[42] The actual value of Δx is arbitrarily chosen. Therefore, the fit parameter ν_0 may deviate from previously published values.
[43] In the total energy landscape, $E = E_s + E_t$, the adatom site slightly deviates from $x = 0$.
[44] R. DiFoggio and R. Gomer, Phys. Rev. B **25**, 3490 (1982).
[45] X. D. Zhu, A. Lee, A. Wong, and U. Linke, Phys. Rev. Lett. **68**, 1862 (1992).
[46] A. Wong, A. Lee, and X. D. Zhu, Phys. Rev. B **51**, 4418 (1995).
[47] L. J. Lauhon and W. Ho, Phys. Rev. Lett. **85**, 4566 (2000).
[48] P. Ohresser, H. Bulou, S. S. Dhesi, C. Boeglin, B. Lazarovits, E. Gaudry, I. Chado, J. Faerber, and F. Scheurer, Phys. Rev. Lett. **95**, 195901 (2005).
[49] F. Ronci, S. Colonna, A. Cricenti, and G. Le Lay, Phys. Rev. Lett. **99**, 166103 (2007).
[50] T. R. Mattsson, G. Wahnström, L. Bengtsson, and B. Hammer, Phys. Rev. B **56**, 2258 (1997).
[51] J. Kua, L. J. Lauhon, W. Ho, and W. A. Goddard, J. Chem. Phys. **115**, 5620 (2001).
[52] A. Dayo, W. Alnasrallah, and J. Krim, Phys. Rev. Lett. **80**, 1690 (1998).
[53] M. Highland and J. Krim, Phys. Rev. Lett. **96**, 226107 (2006).
[54] M. Kisiel, E. Gnecco, U. Gysin, L. Marot, S. Rast, and E. Meyer, Nat. Mater. **10**, 119 (2011).
[55] B. Persson, Solid State Commun. **115**, 145 (2000).
[56] A. Peronio and F. J. Giessibl, Phys. Rev. B **94**, 094503 (2016).
[57] C. Loppacher, R. Bennewitz, O. Pfeiffer, M. Guggisberg, M. Bammerlin, S. Schär, V. Barwich, A. Baratoff, and E. Meyer, Phys. Rev. B **62**, 13674 (2000).